PROCEEDINGS, 41st Workshop on Geothermal Reservoir Engineering
Stanford University, Stanford, California, February 22-24, 2016
SGP-TR-209

New Injection Strategies at Blue Mountain, Nevada Through Tracer Test Analysis, Injection-Production Correlation, and an Improved Conceptual Model

Michael W. SWYER, Matt UDDENBERG, Yini NORDIN, Trenton T. CLADOUHOS, and Susan PETTY

4010 Stone Way North, Suite 400, Seattle WA 98103

tcladouhos@altarockenergy.com

Keywords: tracers, fault permeability, fault modeling, thermal breakthrough

ABSTRACT

The Blue Mountain geothermal field, a fault-controlled geothermal system in the Basin and Range, has been in operation since November 2009. The resource experienced significant temperature decline from an initial operational strategy that focused injection into wells down dip of the production zone. To mitigate the temperature decline, production rate in the fastest cooling well was reduced, which slowed the rate of cooling and decreased power output. This paper describes the strategy started in 2013 of mitigating temperature decline field-wide by adopting an injection management strategy based on the results of tracer testing, a new resource model, and well-to-well correlation of injections rates to production cooling. The resource model is based on fluid conduits and compartments created by the intersection of three west-dipping low angle faults. The fault geometries were fit to lost circulation zones identified during drilling, fluid exit/entry points in wells, and geophysical data - seismic reflection profiles, micro-seismicity, horizontal gravity gradient lineaments, and aeromagnetic data. The intersection between two faults formed a damage zone that creates a high permeability conduit defining the primary up-flow zone fed at depth by a piedmont fault delineated by gravity and seismic reflection on the west edge of the field. A fourth fault that bounds the range to the SW, trends NW and is considered to be a relatively impermeable structure due to its orientation in the current tectonic regime. The conceptual fault model was combined with tracer data to map potential flow patterns at depth, characterize reservoir geometry, and model the thermal behavior of the reservoir. This analysis was used to develop the permeability structure for a reservoir simulator that showed a much better history match than previous models. The new model and tracer analysis also provided the insight to design and implement an injection strategy using existing wells that has slowed temperature decline. Further plans to mitigate temperature decline evaluated by reservoir simulations, include producing some of the initial western injectors and stimulating idle wells further to the north and south.

1. INTRODUCTION

The Faulkner 1 power plant at Blue Mountain began production in November 2009. From 2009 to 2011 the plant inlet temperature declined by more than 10% due to premature thermal breakthrough of cold water injection into what had been the hottest wells on the western edge of the wellfield (57-15, 58-15, and 61-22) (Figure 1). These wells have very strong hydraulic connections to the two hottest production wells at the beginning of plant operation (14-14 and 17-14) confirmed by multiple tracer tests. This initial injection strategy was predicted to flush hot water from the deep western injectors that would increase net power generation and delay thermal breakthrough for 10 years. Instead, high rates of injection into the deep western wells suppressed the up-flow of the highest enthalpy fluids to the wellfield, resulting in extremely high rates of temperature decline. To slow inlet temperature-decline the production rate in well 14-14 was reduced by 50%, which had been the hottest production well and had experienced the greatest temperature decline after startup. Decreasing the production rate in 14-14 reduced the temperature decline rate however it also caused a significant reduction in net power generation.

The decreased power generation warranted a new injection strategy that was implemented in 2012, which involved shutting-in the deep western injectors as much as possible and diverting flow to the injection wells in the northern part of the wellfield. Subsequently, injection flows going to wells 57-15 and 61-22 were reduced and eventually stopped as new injection wells 55-15, 91-15, and 89-11 were brought online, but 58-15 continued to receive high amounts of injection. The shifting of injection has allowed for production in 14-14 to be resumed to its initial rate and eventually increased, causing a modest net generation gain to 85% capacity. However, temperature decline continued at higher rates for the following 2.5 years, and the average net power generation was reduced to 71% capacity.

In addition to diverting injection flows into the heat source in the deep western part of the field, the injection strategy at Blue Mountain was further updated in 2013. The new strategy was informed mainly by analytical modeling of tracer tests as well as correlation analysis of injection/production rates and downhole pressure monitoring of the reservoir. The new strategy included injecting low flows to four wells to the south and east of the current production wells, and one shallow well near the deep western injectors. Due to the complex behavior of the reservoir at Blue Mountain, advanced analysis is needed to reveal non-intuitive well-to-well connections and determine an optimal injection strategy that minimizes temperature decline and provides adequate pressure support.

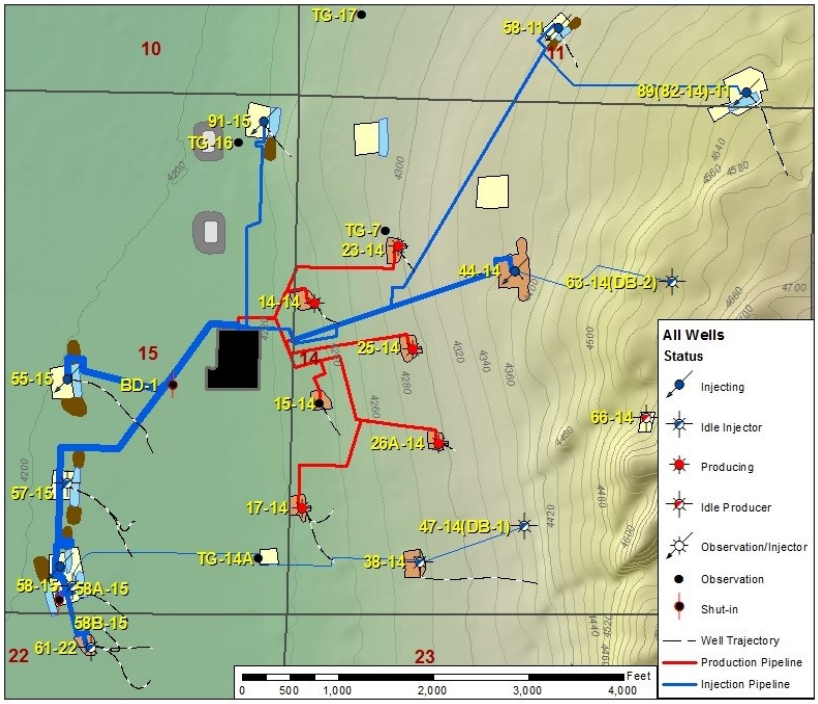

Figure 1: Blue Mountain power plant, wellfield, and piping system with current well status.

The tracer tests, along with downhole temperature logs and mud logs to identify fault crossings, were used to construct a conceptual fault model of reservoir permeability and heat flow. The conceptual model was used to explain the temperature decline and complex subsurface flow patterns, and to update the permeability structure for a reservoir simulation of Blue Mountain first performed in 2012.

2. BACKGROUND

Hot water was first discovered at Blue Mountain during gold exploration activities carried out from 1984-1990, when many of the shallow drill holes encountered temperatures up to 178°F at depths up to 500 ft, with artesian flows up to 20-30 gallons per minute (gpm). In 1994, a geothermal exploration plan was developed for the area that included eleven new shallow drill holes, IP-resistivity surveys, further geologic mapping with interpretation of aerial photographs, and two deep small diameter test holes. In 2002, Deep Blue No.1 (DB-1) was drilled with a maximum temperature of 293°F at a depth of 2,115 ft. In 2004, Deep Blue No.2 (DB-2) was drilled to a total depth of 3,700 ft with a maximum temperature of 333°F at a depth of 1,920 ft and a temperature reversal below that depth. In 2005, DB-2 was deepened to 5003 ft. Drilling these two wells encountered multiple zones of significant lost circulation, which required innovative drilling techniques and lost circulation materials (Petty et al., 2005), to overcome the very high fracture permeabilities encountered in the formations at Blue Mountain.

2.1 Preliminary Structural Analysis

Around the same time that DB-1 and DB-2 were completed, work began on determining a structural geologic model for Blue Mountain. Geologic studies that have been performed at Blue Mountain, which was originally mapped in the mid-1960s, were compiled into a geologic conceptual model. The general lithostratigraphy in the production area is basin sediments overlying phyllitic metasediments with shallow silicic and argillic alteration and diorite intrusions. Studies performed later in the early 1980s to characterize the gold deposits and in the early 2000s to characterize the geothermal resource first revealed a complex deformational history that includes earlier episodes of compression in addition to the more recent Basin and Range extension. Four distinct deformation episodes, known as D1, D2, D3, and D4, were identified at Blue Mountain from mapping done in the range east of the main wellfield (Wyld, 2002), and are thought to be reflected in the reservoir rock under the basin sediments in the production area. D1 is characterized by large scale NW-SE shortening, which produced tight isoclinal ductile folds with axes plunging to the NE. D1 represents the bulk of the strain in the formations at Blue Mountain, and therefore still has some control on the structural grain. D2 was a minor NE-SW contraction which produced some folding, but also brittle cleavage and imbrication in the D1 structures, with cleavage planes trending to the NW. Most of the D2 deformation occurred in the SW part of the range, and has been partially silicified. D3 is an E-W extension event with many N-S trending mafic dykes associated with the diorite intrusions. D4 represents highly localized deformation at Blue Mountain, which formed three distinct faulting trends; 1) left-lateral NE striking faults on the northern edge of the range, 2) left-lateral N-S striking faults in the central and western range area, and 3) right-lateral NW striking faults on the SW boundary of the range, which also represent a major left step in the regional NNE range front fault trend (Szybinski, 2007).

The current Basin and Range extension direction at Blue Mountain is WNW-ESE determined from geodetic strain-rates (Faulds, 2007, references therein). This extension controls the dominant and most prominent fault and fracture directions at Blue Mountain as indicated by four borehole image logs, which have NNE-NE fracture directions in the northern part of the field and a more N-S trending fracture

orientation in the central area of the field near the range front (Peterson and Davatzes, 2012). Like most geothermal fields in the Basin and Range, Blue Mountain occurs at a structural complication where the three fault trends intersect at the western edge of the range front. Most of the fault blocks in the area surrounding Blue Mountain are tilted moderately to the east 20-40°, with Blue Mountain itself tilting 30° to the east (Faulds, 2007) (Figure 2).

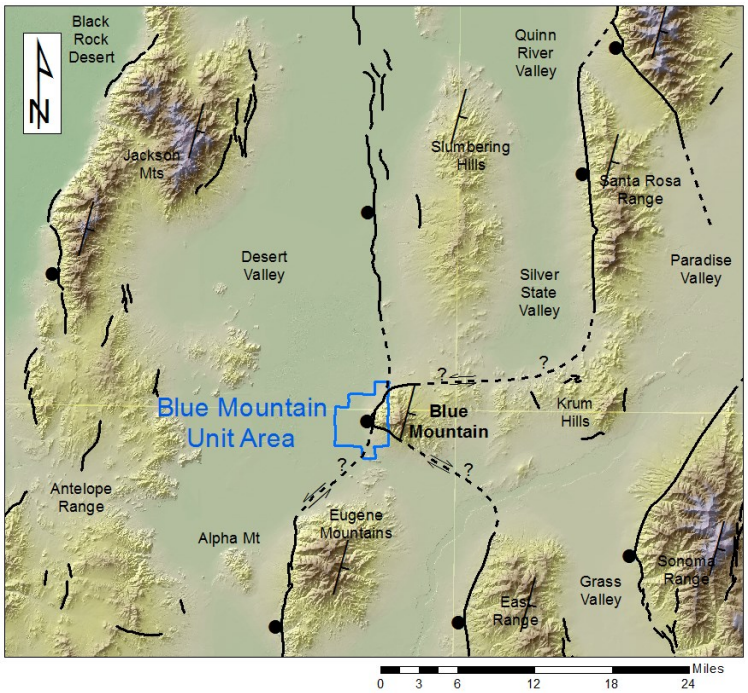

Figure 2: General structure and elevation of area surrounding Blue Mountain. Quaternary faults shown as solid lines and inferred faults buried by sediments shown as dashed lines. Black circles showing westward dip direction of range front faults and strike-and-dip symbols showing eastward tilt of fault blocks (recreated from Faulds, 2007).

2.2 Preliminary Fault Permeability Model

The initial 3D fault model of the reservoir included six steeply dipping faults that connected what was identified as the most permeable zones of all the wells (Melosh et al., 2008). The 3D flow pattern supported by data from temperature gradient wells was first conceptualized as deep convective upward flow of very hot water along Piedmont faults within the range-front fault in the western part of the field. The outflow zone is in the area of the production wells just east of the western up-flow zone, and spreads outward to the north and south. The reservoir also receives meteoric recharge in the range block further to the east. Initial drilling in the western part of the field which was meant to target the up-flow zone for injection also indicated shallow east-dipping permeable structures in the hanging-wall, identified as potential injection targets in addition to the deeper west-dipping up-flow zone (Melosh et al., 2008).

3. UPDATED CONCEPTUAL MODEL AND INJECTION STRATEGY

The multiple episodes of deformation experienced over geologic time justify the use of many faults with varied orientation to represent the permeability structure, but can be better represented by a simpler conceptualization. Changes in the dominant fracture fabric spatially across the field supported by multiple geophysical datasets imply a wrap-around fault pattern parallel to the range front (Figure 3).

An updated fault permeability model is presented in this paper. Instead of multiple parallel faults, the updated model has single fault planes representing each fault trend with a zone of brecciation that is thicker within the fault intersection. This model, like the previous model, is supported by permeable zones in wells, but is further supported by temperature logs indicating the main fluid entry/exit points in the wells, and the most permeable flow paths inferred from tracer testing. The new fault model, tracer tests, and production history were used to implement a new injection strategy which focuses injection to the north and south of the upwelling area, and to the east in the meteoric recharge area, which we believe will provide deeper circulation of hot water and maximize residence time, heat exchange, and reservoir recharge.

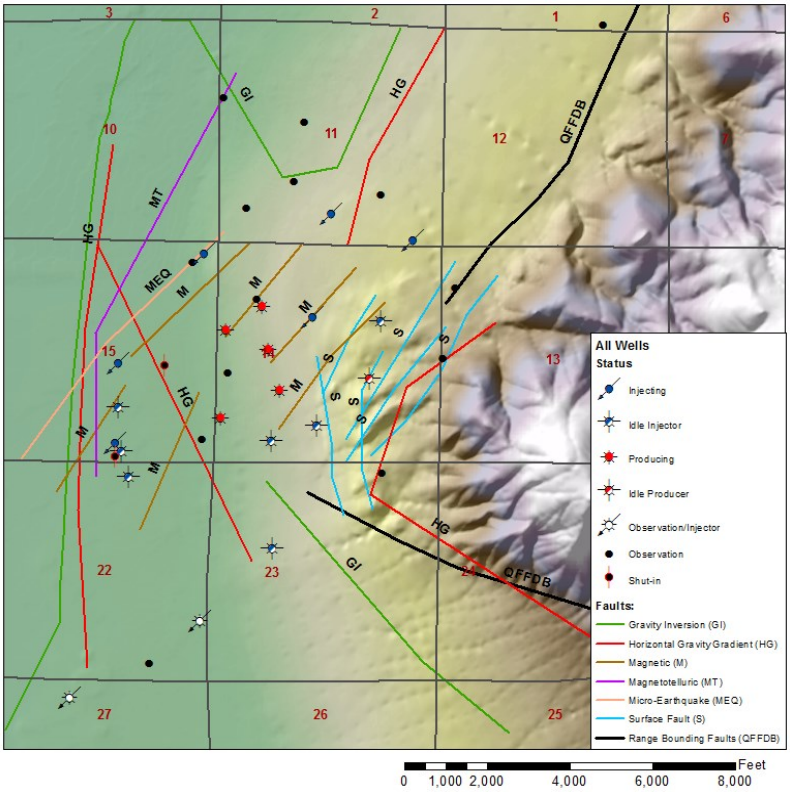

Figure 3: Fault trends interpreted from geophysical data and geologic mapping which show a trend reflective of locally mapped surface faults and regionally defined range front faults from the Quaternary fault and fold database (QFFDB) (geophysical lineations from Engeocon, 2011).

3.1 Fault Geometry

The NE fault trend in the north of the field and the N-S trend in the middle of the field are represented by two fault planes fit to the most permeable zones in two groups of three wells based on the depth of the largest mud losses in the lost circulation zones during drilling (Table 1). Faults were fit to these particular zones of lost circulation rather than all the wells because they are supported by significant temperature gradient changes, temperature reversals, higher flows indicated by spinner logs while injecting, and the most direct connections indicated by tracer data. As is common in geothermal development, the most productive depths of the production wells were drilled blind – that is, no cuttings were recovered – and drilling was stopped before circulation was regained. Thus an estimate of the thickness of the fault zones is based on LCZ in injection wells, which may not be representative of the total thickness of the fault in the most productive areas.

These two planes form an intersection which is postulated to be an extremely high permeability conduit for the major up-flow zone from the deep western part of the reservoir (Figure 4). As a coincidence that partially validates this fault geometry, well 55-15 which was not used to construct the fault model makes contact with the postulated intersection, and has a major zone of lost circulation at that location which had no cutting returns for 690 ft.

Table 1: Two groups of three wells with lost circulation zone (LCZ) points that were fitted with fault planes.

Fault Plane	Well ID	Depth to largest mud loss in LCZ (ft MD)	LCZ Interval (ft MD)
Group 1 Western Fault Strike=188, Dip=40°	14-14	4161	4161-4190
	17-14	3847	3830-3950
	58-15	5603	5580-5706
Group 2 Northeastern Fault Strike=212, Dip=50°	91-15	6605	6555-6670
	58-11	4100	4090-4627
	26A-14	2681	2617-2815
Intersection	55-15	5895	5290-5980 (No Returns)

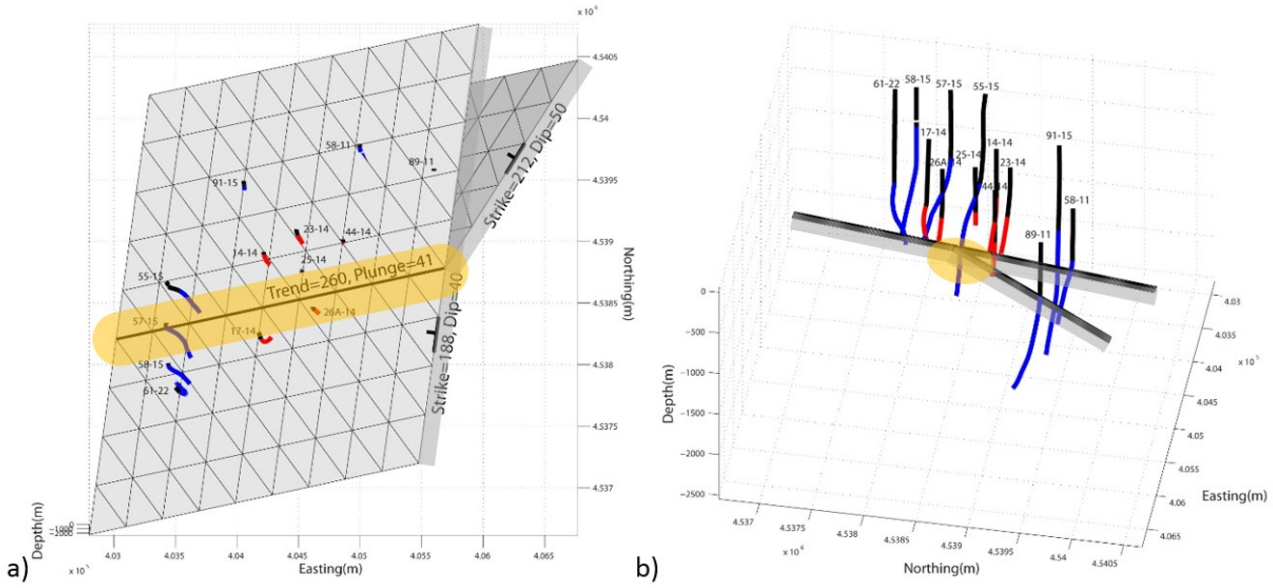

Figure 4: Two fault planes fitted to well LCZs a) map view b) looking down dip (west) along the fault intersection. Planes have assumed brecciation zone thickness in grey, which is thickest near the intersection in yellow based on 690 ft LCZ in 55-15, which penetrated the full thickness of the fault zone.

The modeled faults have shallower dips (40-50°) than the previous fault model (Melosh et al., 2008), and than "typical" Basin and Range normal faults. The 30° eastward tilt of the Blue Mountain block observed in bedding attitudes could indicate domino-style block rotation of the range which also rotated the faults to a lower angle than initial formation. The shallower dips are also consistent with measured attitudes on outcropping faults to the north and east of the well field (Faulds, 2007).

These fault planes represent the 3D geometry of the highest permeability flow paths observed in the wellfield. A more complete version of the fault geometry model includes the Southeastern fault, a NW trending fault that bounds the SW edge of Blue Mountain, and a N-S trending steeply-dipping Piedmont fault in the deeper, western part of the wellfield (Figure 5). Unlike the Western and Northeastern

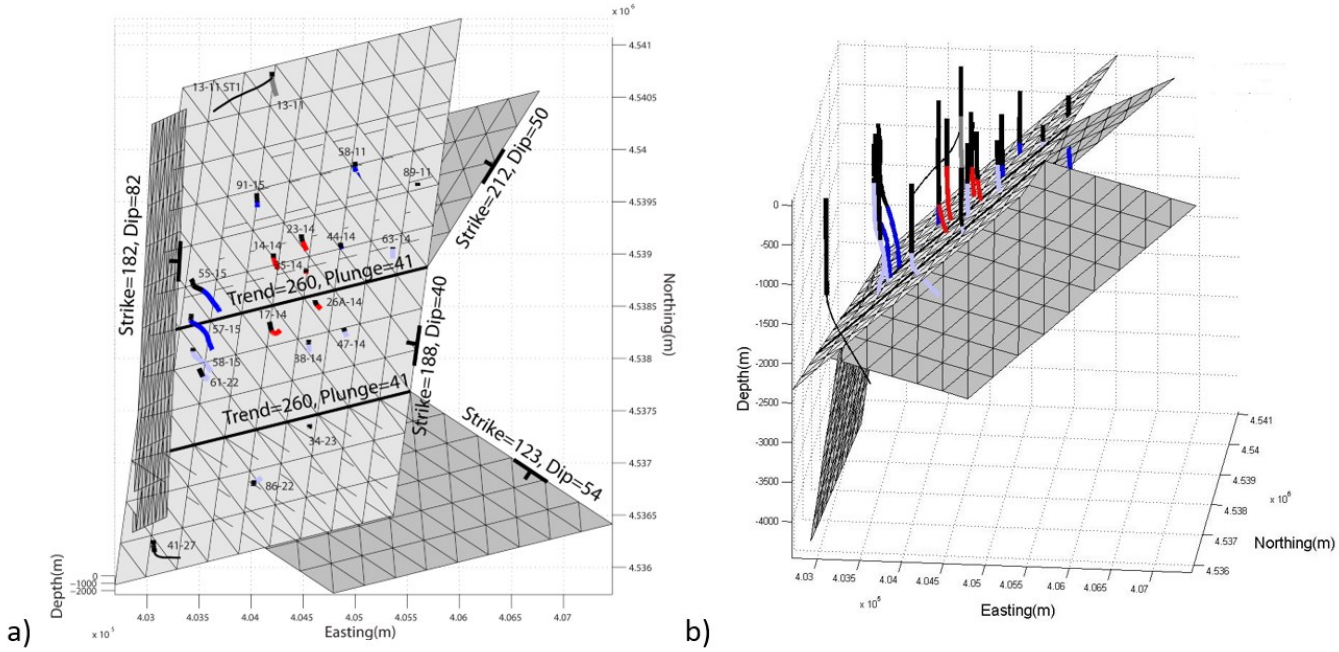

Figure 5: Fault geometry model at Blue Mountain including faults inferred from geophysics a) map view b) looking north. Planes show top of fault zone with ~500 ft thickness.

faults which are intersected by well-bores (Table 1), these two faults were inferred from horizontal gravity gradient lineaments (EDCON, 2008) (Figure 3) and the Quaternary fault trace of the SW range front fault. The Piedmont fault was also modeled partially

from seismic reflection profiles (Optim, 2007), however, the velocity model is not well constrained at the depths of interest for the Piedmont fault, and the quality may have been affected by ground roll noise (Cummings, 2008). The Piedmont fault is the source of up-flow and heat for the reservoir and hydraulically connects to the producing faults through the intersection. The NW trending fault represents a flow barrier because of its low slip tendency due to its orientation relative to the current WNW-ESE extension direction, and is most likely the reason why the wells to the south are impermeable from hydrothermal mineral deposition/cementation causing very weak connections to the central wellfield.

The following sections describe how this model was used to explain some of the complex flow paths inferred from tracer testing, and how it has been an effective baseline for the permeability structure in numerical modeling.

3.2 Tracer Testing

On three separate occasions, injection wells at Blue Mountain were tagged with uv-fluorescent naphthalene sulfonate tracers, which are thermally conservative and environmentally benign (Rose et al., 2001; Greim et al., 1994): 1) 2009 shortly after wellfield/plant operations began in the first three western injectors (61-22, 58-15, 57-15) and a well to the east originally intended for production (44-14), 2) 2010 after three new injectors in the north came online (55-15, 91-15, and 58-11), and 3) 2012 after a fourth northern injector came online (89-11). Careful analysis of this data has been invaluable for allocating injection in the wellfield to effectively manage the resource and minimize thermal breakthrough. Tracer connections were mapped with normalized weights based on peak concentrations and arrival times, and injection/production rates:

$$WF = \frac{C_{peak}}{T_{peak}\left(Q_{inj} + Q_{prod}\right)/2} \quad (1)$$

Where WF is the weighting factor, C_{peak} is the peak concentration, T_{peak} is the time to peak concentration, and $Q_{inj/prod}$ are injection and production rates for each well pair. Then, conjectural flow patterns were inferred from the relative peak concentrations and arrival times in the production wells. Reservoir geometry was characterized by first temporal moment analysis (Shook and Forsmann, 2005) and thermal breakthrough analysis (Shook, 2001) developed at the Idaho National Laboratory to determine 1) mean residence time 2) reservoir swept pore volume 3) percent tracer recovery to assess connectivity, 4) flow-storage capacity, or F-C diagram to assess capacity for heat exchange, and 5) time to normalized thermal breakthrough. F-C diagrams show how much a well to well connection has strayed from idealized homogeneous porous medium by flowing through a smaller number of large fractures/faults, and thermal breakthrough is similar to accumulated recovery of total tracer injected with a modeled thermal drawdown based on the rock/water properties listed in Table 2.

Table 2: Rock properties used in thermal breakthrough formulation from Shook, 2001.

Parameter	Value
Porosity	0.05
ρ_{rock}	2.71 g/cc
ρ_{water}	0.89 g/cc
Rock Heat Capacity	1 KJ/Kg°C
Water Heat Capacity	4.4 KJ/Kg°C

3.2.1 Tracer Test, December 2009

Tracer return curves are plotted by injector in Figure 6, and flow patterns are mapped in Figure 7. All three western deep injectors have fast and strong peaks at 14-14 followed by weaker concentrations in 17-14, except for 57-15 which connects to 14-14 first but at half the concentration as the other two wells, and has a stronger connection to 17-14. These levels of tracer concentration (>100 ppb) with such rapid arrivals (5-15 days) are why these two production wells experienced the highest rate of decline after production began. There is also evidence of reservoir compartmentalization in this test. The fast and strong arrivals in 14-14 and 17-14 are followed by weaker arrival in 23-14, then a delayed but stronger connection to 25-14, and finally a gradual rise in 26A-14. This suggests that the western producers 14-14 and 17-14 are in a separate compartment from the eastern producers 23-14 and 25-14, and that 26A-14 may be in a separate compartment of its own. The separation of 26A-14 is further supported by the tracer from 44-14, which has a fast and strong arrival to 26A-14 followed by a weaker and delayed return in 17-14.

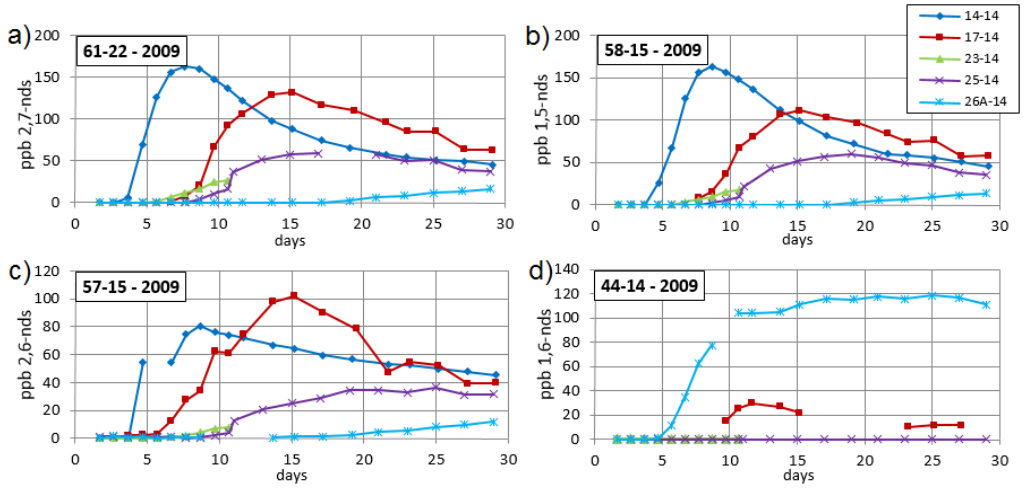

Figure 6:Tracer return curves by tagged injector for 2009 test from a) 61-22, b) 58-15, c) 57-15, and d) 44-14.

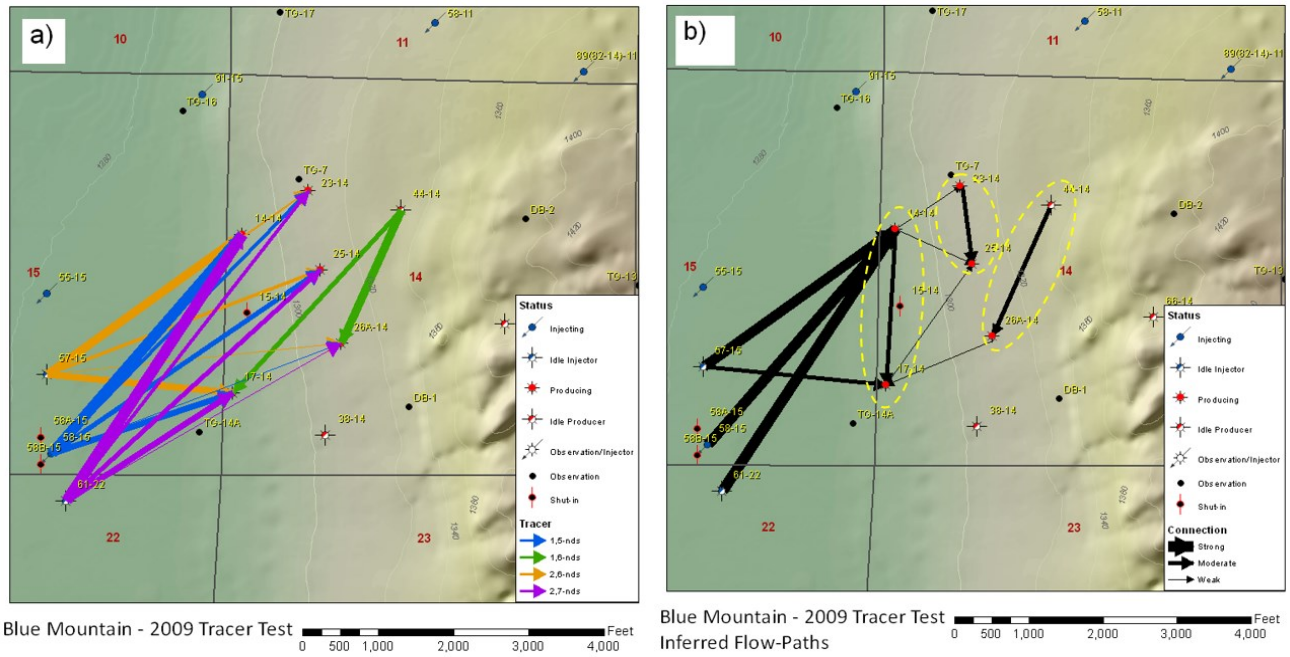

Figure 7: a) Mapped injection-production weights from equation (1) and b) conjectural flow patterns with apparent reservoir compartments outlined with dashed yellow ovals.

Most of these well connections have high pore swept volumes (>50,000 m^3) and low mean residence times (<35 days). The F-C curves (Figure 8a) and thermal breakthroughs (Figure 8b) indicate direct subsurface connections to the production wells, meaning their high swept pore volumes are contained in large fractures/faults rather than smaller fractures and/or porous rock. The eastern production wells (23-14, 25-14 and 26A-14) have very little connectivity to the injectors tagged in this tracer test because less than 10% tracer was recovered in these wells, which means the injection scheme of late 2009 was ineffective for evenly distributing fluids across the wellfield. The exception was the too strong connection between the only injector on the east, 44-14, and 26A-14, which also caused cooling in the producer. The injectors that have more tortuous flow paths and lower levels of thermal breakthrough are 44-14 and 57-15, so moderate amounts of injection to these wells would cause less thermal decline than 61-22 and 58-15.

The primary conclusion of the 2009 tracer tests was that the western injectors (61-22, 57-15 and 58-15) were far too well connected to the western producers (14-14 and 17-14), which had started as the hottest two wells in the field. This problem soon became critical as the western producers rapidly cooled, requiring a new injection strategy in wells along fault strike, rather than down-dip.

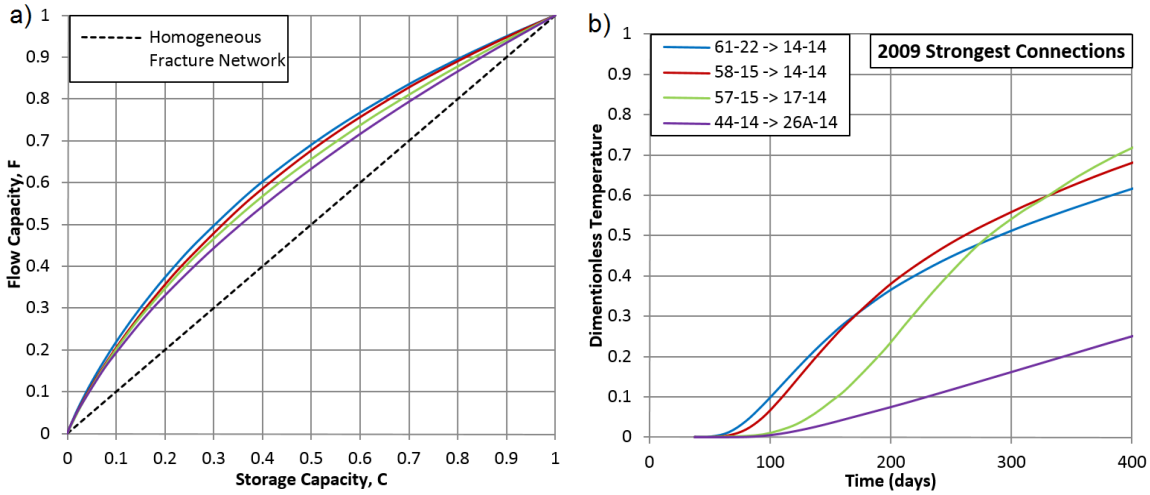

Figure 8: a) F-C plot and b) thermal breakthrough for the strongest well to well connections in 2009.

3.2.2 Tracer Test, August 2010

While none of the wells tagged in 2009 had a strong connection to production well 23-14, the three wells tagged in 2010 (91-15, 55-15, and 58-11) do provide recharge to 23-14, and to the eastern producers in general (Figure 9). The 2010 tracer test data was particularly useful for diagnosing the high rates of temperature decline in 23-14 and 25-14 that occurred after production rates were increased in 2013 by restricting injection to 58-11, which has the strongest connection to those two wells (Figure 10). 91-15 and 55-15 have moderate to high levels of connectivity to the production wells, but not as high as 58-11 and the other deep western injectors tagged in 2009.

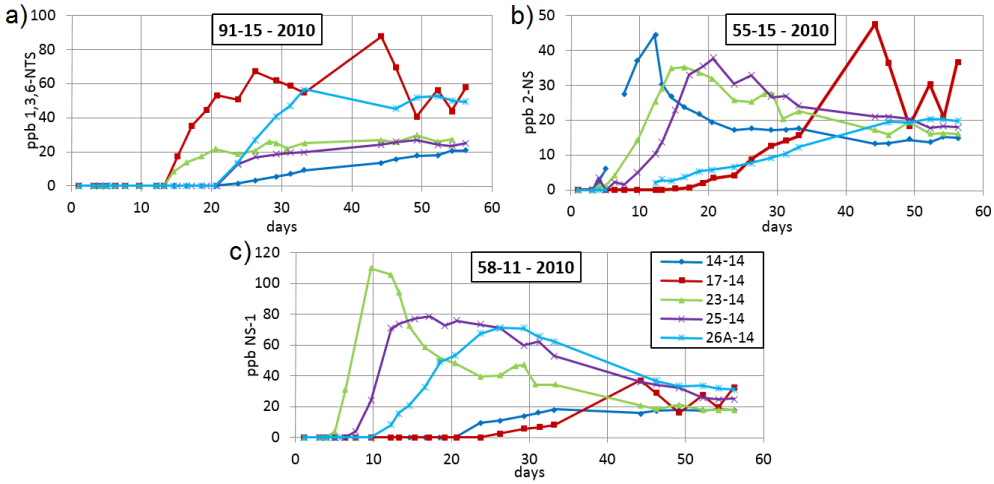

Figure 9: Tracer return curves by tagged injector for 2010 test from a) 91-15, b) 55-15, and c) 58-11.

The tracer pathway that swept the largest pore volumes (90,000-250,000 m^3) and had the longest residence times (50–200 days) came from 55-15 indicating that it is a very good injector. However the fast (12 day) break-through to 14-14 may become problematic in the long term. The most tortuous flow-path to the production wells is from 91-15. The other two wells are more direct and have very similar F-C curves (Figure 11a). The generally high pore swept volumes and residence times, and moderate tracer recovery (10-60%) of all these tracer tests suggests that 55-15, 58-11 and 91-15 are good injectors with fracture pathways that provide good pressure support and recharge but will not cause excess cooling.

The primary conclusion of the 2010 tracer testing was that significant progress had been made in implementing an injection strategy that would at least partially mitigate the early rapid cooling experienced in the field. However, it was also clear that additional adjustments had to made, including complete shut-in of the western injectors except 55-15 which would require finding additional injection capacity and reducing flow to 58-11 to prevent excessive cooling of 23-14 and 25-14.

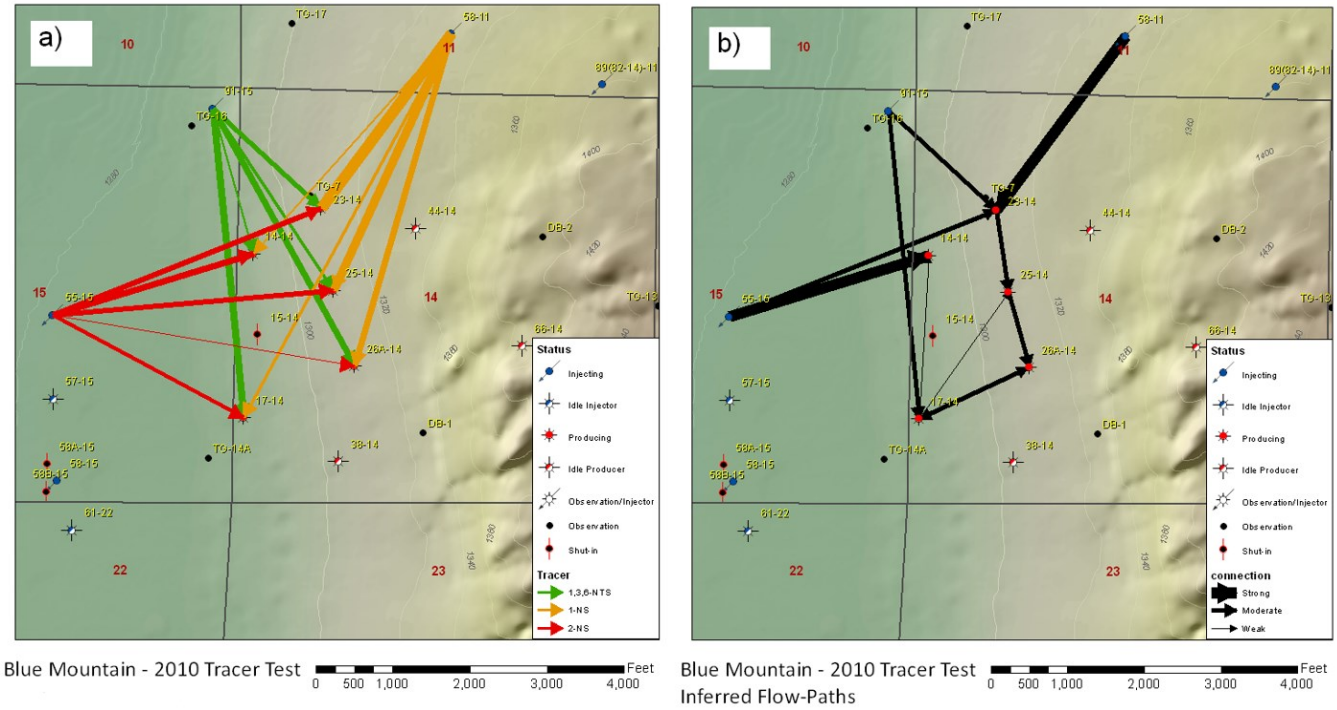

Figure 10: a) Mapped injection-production weights from equation (1) and b) conjectural flow patterns.

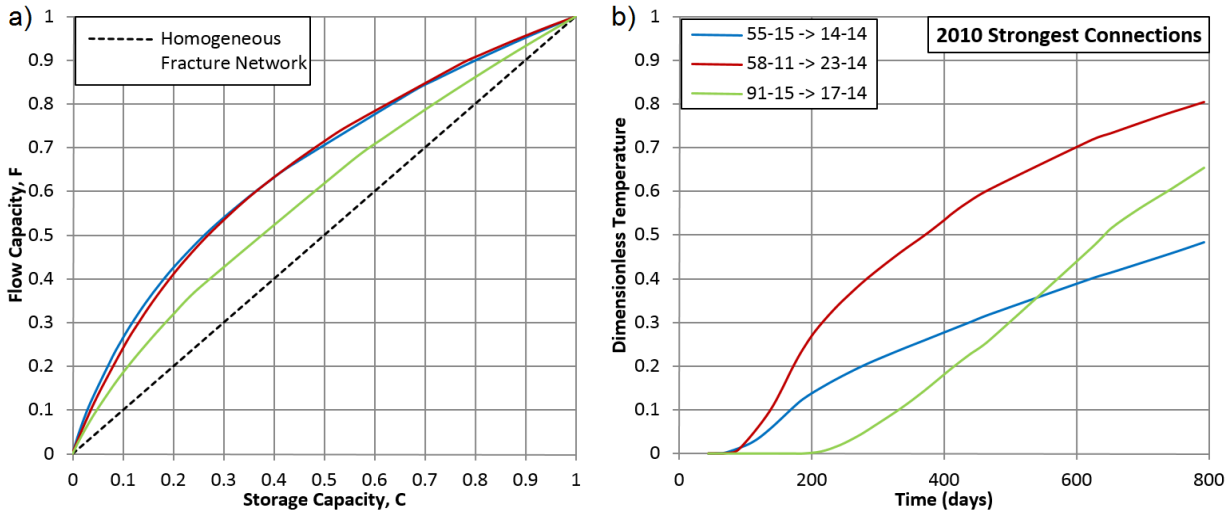

Figure 11: a) F-C plot and b) thermal breakthrough for the strongest well to well connections in 2010.

3.2.3 Tracer Test, April 2012

A new injector, 89-11, was brought online in mid-January 2012, thus a third tracer test was performed in April of 2012 to measure the new injector's impact on the producers. The tracer from 89-11 seems to have a clear breakthrough at all the production wells after 40-50 days; however, the coincidence of a peak for all five production wells points to a laboratory issue related to the 1,3,6 nds tracer injected to 89-11, perhaps interference with other tracer species in those samples (Rose, pers. comm., 2013) (Figure 12a). Therefore, it appears that injection to 89-11 requires more than 80 days to return to the production wells, which makes it a very good injector unless there are no returns. A fourth tracer test, with sample collection of at least 120 days, will be needed to confirm.

The return curves from 58-15 closely resemble those from 2009, except that the peak concentrations are even higher (Figure 12d). Three of the production wells recovered over 100% tracer from 58-15, which means this data needs to be de-convoluted to remove re-injected tracer that has been recycled through the reservoir (Rose et al., 2004).

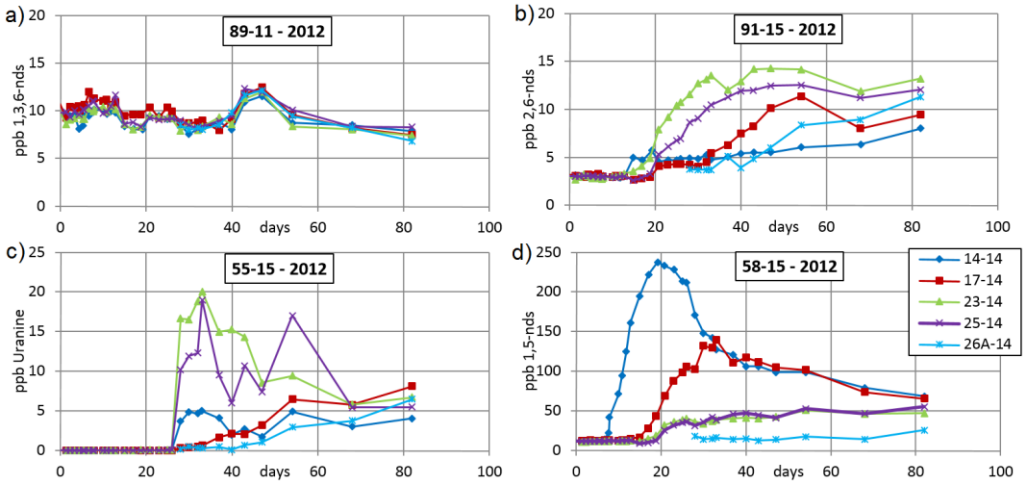

Figure 12: Tracer return curves by tagged injector for 2012 test from a) 89-11, b) 91-15, c) 55-15, and d) 58-15.

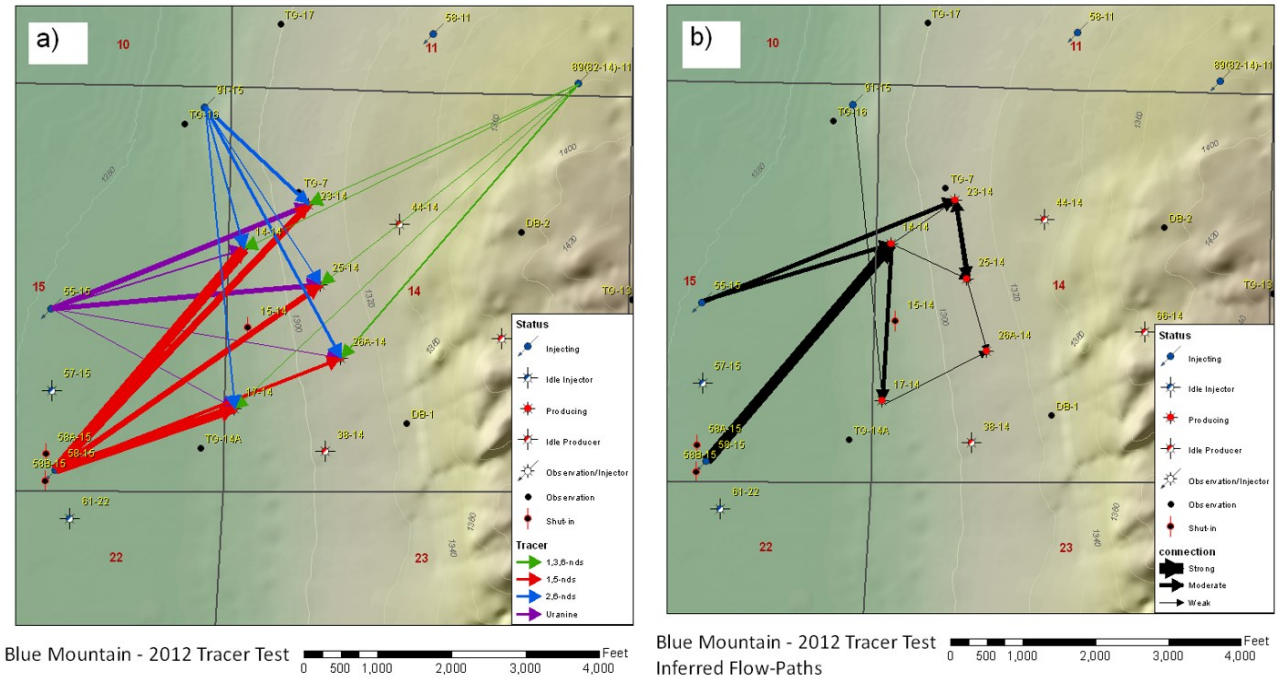

Figure 13: a) Mapped injection-production weights from equation (1) and b) conjectural flow patterns.

Tracer concentrations from 91-15 and 55-15 are significantly lower than 2010 and their flow-paths through the reservoir have changed. From the F-C plot it becomes clear that 55-15 and 91-15 are the best injectors, with 55-15 being slightly better (Figure 14a), although this well has a stronger thermal breakthrough (Figure 14b). The results from 2010 and 2012 tracer tests provide a useful resource management tool for Blue Mountain. Careful allocation of injection to these two wells could help maintain the distribution of flow to areas that need it, or withhold flow from areas that do not.

The primary conclusions of the 2012 tracer test was that 58-15 had to be shut-in as soon as possible due to continued rapid breakthrough. The injectors at the northern edge of the field (55-15, 91-15 and 89-11) continued to be good injectors, although the flow patterns from 55-15 and 91-15 have changed from 2010, and the connectivity, pressure support, and recharge provided by 89-11 is still unknown.

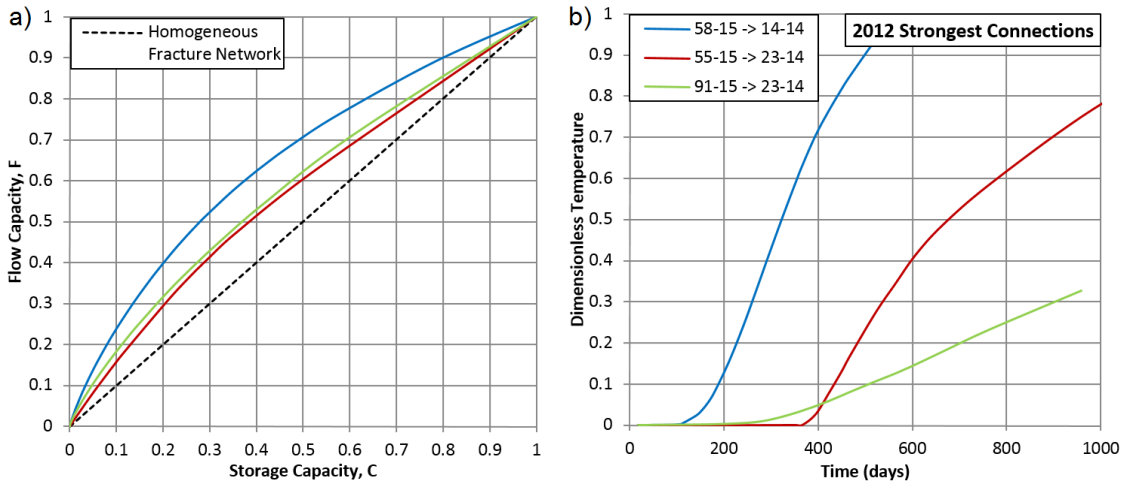

Figure 14: a) F-C plot and b) thermal breakthrough for the strongest well to well connections in 2012.

3.2.4 3D Flow Paths

The conjectural flow-paths inferred by tracers can also be explained by the reservoir elevation described by the conceptual fault model. In 2009, when the deep western injectors were used, production wells with deeper fault intersection tended to receive fluid from the deep western injectors first, implying that the western injectors are cooling the upwelling fluid in the reservoir from the bottom and flowing upward along the fault conduit system (Figure 15). Wells that inject into the fault system at similar or higher elevations connect better horizontally to wells across the damage zone, but do not have strong connections to wells at lower elevations because of reservoir pressure and upward flow from the western and northwestern deep injectors may prevent the cooler injected fluid from sinking (Figure 16).

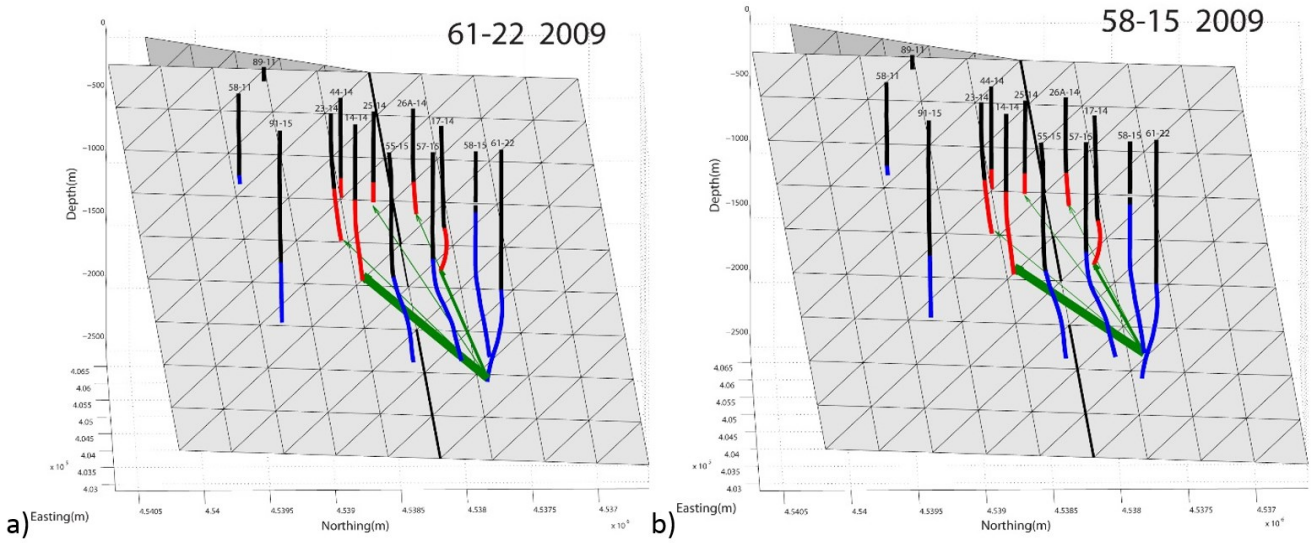

Figure 15: Tracer tests from 2009 in deep western injection wells a) 61-22 and b) 58-15. Line thicknesses are based on the relative peak tracer concentration, arrival times, and injection/production rates in the wells. These are two examples of deep injectors cooling the fault system from the bottom up.

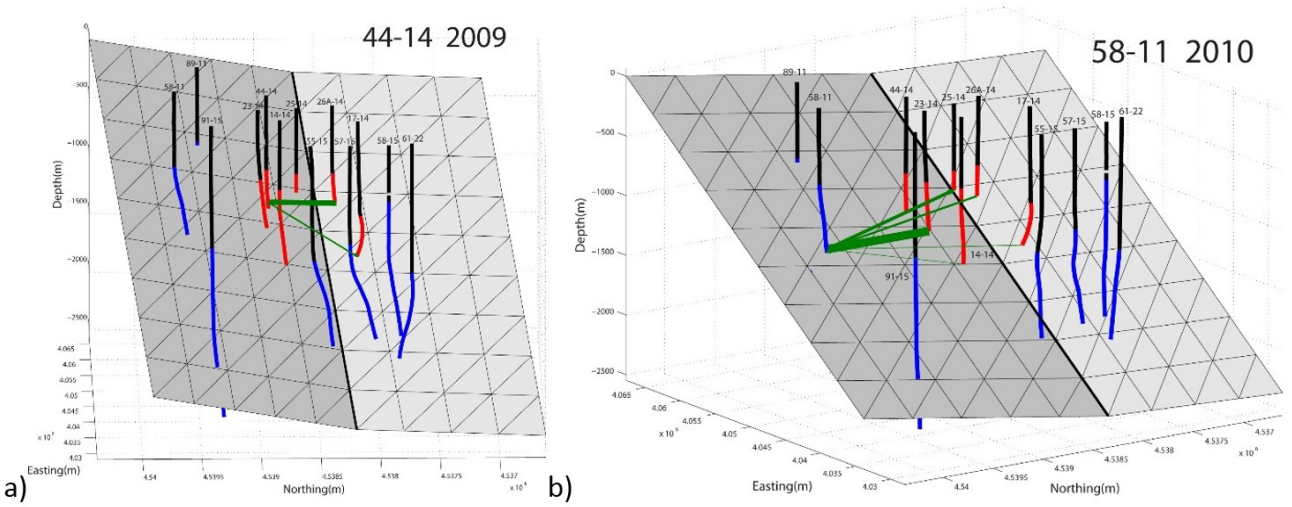

Figure 16: Tracer tests from a) 2009 in then injection well 44-14 b) 2010 in injection well 58-11. Line thicknesses are based on the relative peak tracer concentration, arrival times, and injection/production rates in the wells. These are two examples of shallow injectors that have stronger lateral flow components with weaker connections to production wells at lower elevations.

3.3 Numerical Modeling

The permeability structure for a geothermal reservoir simulator originally developed by Geothermal Science, Inc. (GSI, 2012) was updated based on the new conceptual fault model (Figure 17). Previous iterations of the permeability structure performed by GSI implied a singular up flow zone at depth to the west, but this behavior was not explained by the previous geological. By implementing the new permeability structure as a baseline for model iteration and calibration, the new simulations of the Blue Mountain reservoir created a better fit to historical production and tracer data (Figure 18) (Holt and Murphy, pers. comm., 2015).

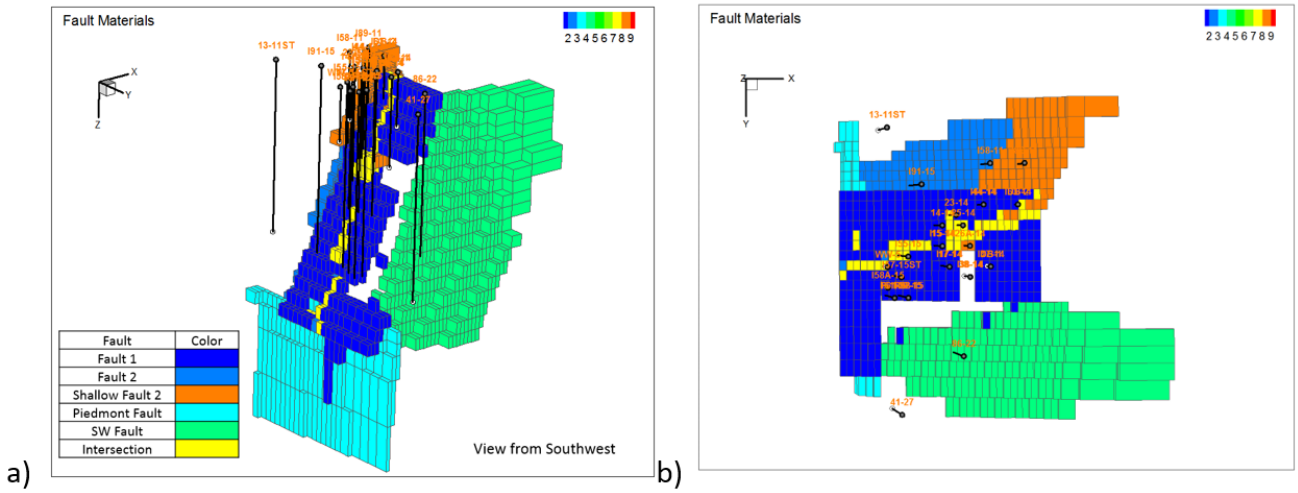

Figure 17: Permeability structure based on the conceptual 3D geologic model implemented into the reservoir simulator by GSI a) view from SW and b) map view.

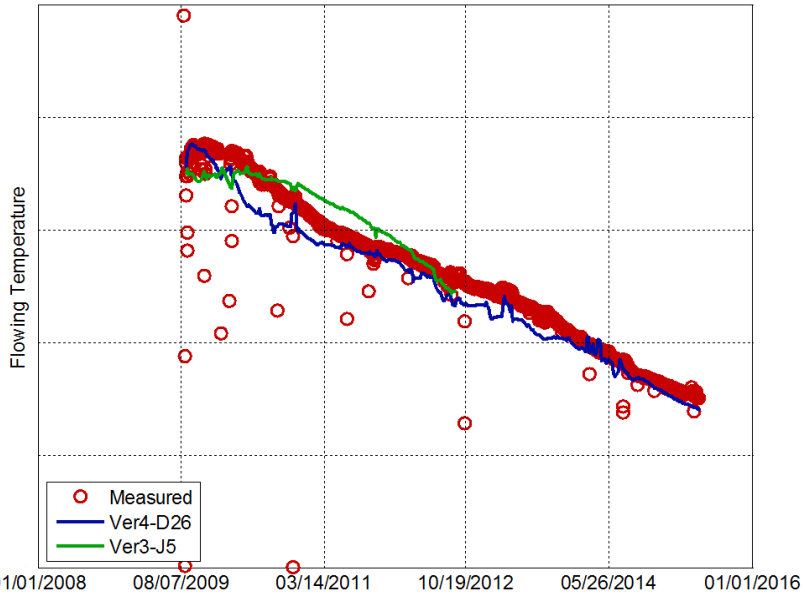

Figure 18: Fit to field wide historical temperature data in previous reservoir simulation run in 2012 (Ver3-J5) and reservoir simulation using new reservoir permeability structure (Ver4-D26).

3.4 Trickle injection

Based on the conceptual model and tracer analysis results, a campaign of low-flow 'trickle' injection was tested to find additional injection capacity for the wellfield in order to shut-in the western injectors completely. Less than 300 gpm per injector was diverted to wells with existing injection piping (38-14 and 58A-15), existing production piping (44-14), or wells that required installation of temporary injection lines (DB-1 and DB-2). Injection rates were restricted for these wells because they were known to cause high levels of cooling, or did not provide necessary pressure support. Coreholes DB-1 and DB-2 were permitted for temporary injection for one month. Both coreholes had commercial grade injectivity with no observable cooling or drawdown effects. In 2011, injection to 38-14 was briefly attempted but caused a temporary high rate of cooling in 26A-14 – fortunately, the temperature in 26A-14 recovered when injection to 38-14 was stopped. This behavior was confirmed by a short re-test in 2014. In 2009, tracer testing showed that 44-14 had a strong connection to 26A-14 followed by a weak connection to 17-14. Since 2014, injection into 44-14 has been kept below 300 gpm, a rate that does not cause significant cooling in 26A-14 nor 17-14. In the past, injection at high rates into 58A-15 significantly reduced pressure support and caused drawdown in the reservoir. In 2015, low injection rates into 58A-15 has not resulted in reservoir drawdown. Keeping 44-14 and 58A-14 under injection at low flows has allowed all three of the deep western injection wells (57-15, 58-15 and 61-22) to be shut in, and lessened the temperature decline to 30% of its initial rate (Figure 19).

4. CONCLUSION/FUTURE WORK

The simpler updated 3D geologic model is consistent with lost circulation zones observed in deep wells, temperature and flow anomalies from temperature and spinner logs, well connectivity revealed by tracer test results, and pressure/temperature responses to operational changes. Updated numerical modeling using the new conceptual model has provided a better history match to field production and tracer data. The combined efforts of the conceptual model, in-depth tracer test analysis, and numerical modeling results allowed the operator to optimize the field by shifting injection away from the initial western injectors and utilize idle wells as trickle injectors to minimize production temperature decline. To date, the Blue Mountain plant is able to reduce overall temperature decline by 70% compared to the initial rate of decline observed in 2009-2011. The change of injection strategy at Blue Mountain has most likely caused drastic changes in subsurface flow patterns. In addition, a small number of wells (2-3) have had injectivity increases while under long term injection and are suspected to have been stimulated. These changes warrant additional field-wide tracer tests to determine what the new subsurface flow patterns are in the reservoir, and confirm suspected new connections that have been created from stimulation. A fourth tracer test will include another temporary permit for DB-1 and DB-2 to determine if they are viable for completion and permitting as permanent injectors. Recently, a flow test of one of the deep western injectors has shown promising flow and heat-up results. Injection capacity for the additional production flow from one or two new production wells to the west will be accommodated by stimulating three idle far-field wells north and south of the currently active wellfield.

Ongoing collaborative efforts at Blue Mountain are also being carried out to improve knowledge of reservoir connectivity and structure. Analysis of stable and clumped isotope geochemistry of calcite in well cores and cuttings by the University of Washington will be used in a methodology developed to assess fracture connectivity across geothermal reservoirs (Sumner et al., 2015). A seismic monitoring campaign at Blue Mountain in 2010 was used partially to validate the fault model, and to monitor subsurface flow patterns as injection was shifted to the north (Casteel, 2010). A new seismic monitoring campaign in collaboration with the Los Alamos National Laboratory is in progress, and will continue those efforts by improving the velocity model, refining the structural model, and determining patterns of subsurface flow.

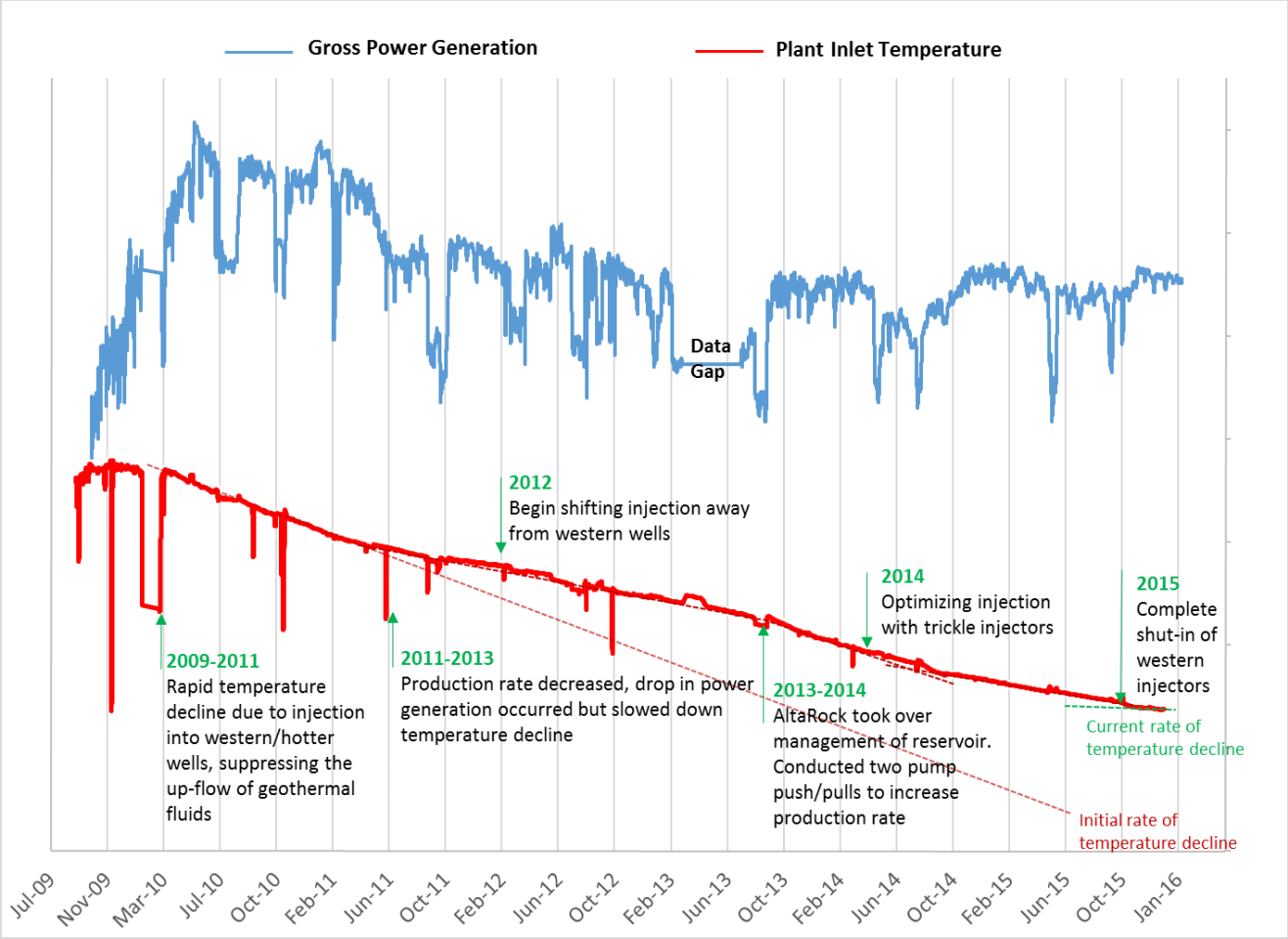

Figure 19: Blue Mountain historic performance data. Red line documents the plant inlet temperature over time, reflecting the injection/production strategies operators took over time in order to mitigate thermal decline. Current thermal decline is 30% of its initial rate. Blue line displays the gross power generation over time. Generation has been mostly stable since 2015 due to a series of field and plant optimizations performed.

REFERENCES

Casteel, J.: Review and Interpretation of MEQ Results: Blue Mtn. March-October, (2010).

Cumming, W.: Review of Blue Mountain Active Seismic Data, for Nevada Geothermal Power Inc. (2008).

EDCON: Interpretation of Detailed Land Gravity, Blue Mountain Geothermal Project, Humboldt and Pershing Counties, Nevada, for Nevada Geothermal Power Inc. (2008).

ENGEOCON: Resource Evaluation and Review of Resource Data, the Blue Mountain Geothermal Project, Humboldt County, Nevada, for Nevada Geothermal Power Inc. (2011).

Faulds, J.E.: A Preliminary Structural Model for the Blue Mountain Geothermal Field, Humboldt County, Nevada, Nevada Bureau of Mines and Geology (2007).

Geothermal Science, Inc.: Numerical Model of the Blue Mountain Geothermal Field-Development and Preliminary Results, for EIG Global Energy Partners (2012).

Greim, H., Ahlers, J., Bias, R., Broecker, B., Hollander, C., Gelbke, H.P., Klimisch, H.J., Mangelsdorf, I., Paetz, A., Schön, N., Stropp, G.: Toxicity and ecotoxicity of sulfonic acids: structure-activity relationship. *Chemosphere*, Vol. 28, p. 2203-2236 (1994).

Melosh, G., Casteel, J., Niggeman, K., Fairbank, B.: Step-Out Drilling Results at Blue Mountain, Nevada, Geothermal Resources Council *Transactions*, Vol. 32, p. 49-51 (2008).

Optim: Final Technical Report, Active Source Seismic Exploration and Development at the Blue Mountain Geothermal Project, Humboldt County, Nevada (2007).

Peterson, S.P., Davatzes, N.C.: Blue Mountain Image Log Analysis, Summary of Preliminary Results, Temple University (2012).

Petty, S., Fairbank, B., Bauer, B.: Lessons Learned in Drilling DB-1 and DB-2 Blue Mountain, Nevada, *Proceedings,* 13th Workshop on Geothermal Reservoir Engineering, Stanford University, Stanford, CA (2005).

Rose, P.E., Benoit, W.R., Kilbourn, P.M.: The Application of the Polyaromatic Sulfonates as Tracers in Geothermal Reservoirs, *Geothermics*, Vol. 30, p. 617-640 (2001).

Rose, P.E., Mella, M., Kasteler, C., Johnson, S.D.: The Estimation of Reservoir Pore Volume from Tracer Data, *Proceedings*, 29th Workshop on Geothermal Reservoir Engineering, Stanford University, Stanford, California, January 26-28 (2004).

Szybinski, Z.A.: Report on Revised Structural Setting of the Blue Mountain Geothermal Project Area Humboldt County, Nevada, for Nevada Geothermal Power Inc. (2007).

Shook, M.G.: Predicting Thermal Breakthrough in Heterogeneous Media from Tracer Tests, *Geothermics*, Vol. 30, n. 5, p. 573-589 (2001).

Shook, M.G., Forsmann, J.H.: Tracer Interpretation using Temporal Moments on a Spreadsheet, INL/EXT-05-00400 (2005).

Sumner, K.K., Camp, E.R., Huntington, K.W., Cladouhos, T.C., Uddenberg, M.: Assessing Fracture Connectivity using Stable and Clumped Isotope Geochemistry of Calcite Cements, *Proceedings*, 40th Workshop on Geothermal Reservoir Engineering, Stanford University, Stanford, California, January 26-28 (2015).

Wyld, S.J.: Structural Evolution of a Mesozoic back-arc fold-thrust belt in the U.S. Cordillera: New Evidence from Northern Nevada, Geologic Society of America, *Bulletin*, Vol. 111, p. 17-38 (2002).